Original Article

Hybrid controller of magnetorheological semi-active seat suspension system for both shock and vibration mitigation

Xian-Xu 'Frank' Bai⑩ and Sen Yang

Abstract

The impact caused by the detonation of landmines and improvised explosive devices may directly lead to spine fracture and injury of seated occupants on special vehicles. The vibration transmitted from the uneven road surface is another important factor affecting ride comfort/health, on the other hand. Aiming at minimizing the injury to spine and "discomfort" due to the shock and vibration from the terrain or blast, a magnetorheological (MR) energy absorber (EA)–based semi-active seat suspension system for both shock and vibration mitigation is proposed and investigated in this article. The proposed MR semi-active seat suspension system consists of a coil spring supporting the seat and the occupant, a MREA, and a fail-safe EA rod. The dynamic model of the MR semi-active seat suspension system with a 4-degree-of-freedom lumped-parameter model for seated occupant is established. A concept of integrated hybrid controller combining strategies for shock and vibration control is proposed and designed. The hybrid controller employs the skyhook control strategy to achieve vibration control and the "soft-landing" control strategy to achieve shock control, and it switches between the two control strategies according to the system dynamic states. Based on the real-time velocity of the seat, the motion process of the "vehicle-seat-human" system can be pre-judged, and the critical point for switching the two control strategies can be determined. A feedforward control strategy based on a hysteresis model with a resistor-capacitor (RC) operator is proposed and realized to high-efficiently output desired damping force of the hybrid controller from the employed MREA. Sequentially, both ride comfort (i.e. vibration control) and vertical safety (i.e. shock control) of the MR semi-active seat suspension system are analyzed and evaluated under different excitations.

1. Introduction

The explosion shock of landmines and improvised explosive devices threats seriously to the safety of the seated occupants on special vehicles. For a long time, researchers, manufacturers, and special vehicle users have been focusing on the protection of the special vehicles themselves (i.e. the special vehicles should not be broken down during explosions). With the improvement of the vehicle protection techniques, although the number of casualties decreased significantly, the number of spine injuries increased much due to the "impact effect" (Radonić et al., 1994, 2004). The "impact effect" is defined by the process of the special vehicles falling back to the ground after being blown up to the air. Such process will generate a huge impact acceleration and act on the human body (spine). At the same time,

the special vehicles run on potholed and fluctuated terrain, and the frequency of the induced vehicle vibration is basically less than 10 Hz, which covers the human's vertical sensitive frequency range (ISO, 1997; Li et al., 2012). The improvement in ride comfort could be achieved by improving the vibration attenuation performance of the vehicle suspensions (Nieto et al., 2016;

Laboratory for Adaptive Structures and Intelligent Systems (LASIS),
Department of Vehicle Engineering, Hefei University of Technology, Hefei,
People's Republic of China

Corresponding author:
Xian-Xu 'Frank' Bai, Laboratory for Adaptive Structures and Intelligent
Systems (LASIS www.lasiser.com), Department of Vehicle Engineering,
Hefei University of Technology, Hefei 230009, People's Republic of China.
Email: bai@hfut.edu.cn

Uys et al., 2007; Zuo and Zhang, 2013), but trade-off between the handling stability of the vehicles and the ride comfort must be made. For the special vehicles, as compared to the ride comfort performance, the handling stability is the more focused performance (Els et al., 2007; Hui, 2011).

Seat suspensions are the components installed between the floor and the seated occupants. Improving the vibration and shock mitigation performance of the seat suspension systems is an effective way to enhance ride comfort and reduce the probability of occupants' physical fatigue and spine injury (Bai et al., 2017a; Hiemenz et al., 2007; Sun et al., 2016). In the field of vibration control for active or semi-active seat suspension systems, so far, many references (Choi et al., 2000; Choi and Han, 2007; Du et al., 2011, 2018; Ning et al., 2016, 2018; Patil and Palanichamy, 1988; Phu et al., 2015, 2017, 2018a, 2018b; Shin et al., 2016; Sun et al., 2011, 2015; Wang et al., 2016; Yu et al., 2018; Zhao et al., 2010) could be found on the structural design and corresponding control strategies. Choi's group (Choi et al., 2000; Choi and Han, 2007; Phu et al., 2015, 2017, 2018a, 2018b; Shin et al., 2016) proposed control strategies to improve vibration attenuation performance of semi-active seat suspension systems equipped with electrorheological (ER)/magnetorheological (MR) energy absorbers (EAs). Combining the robustness of H∞ and sliding mode control strategies and no requirement of accurate system model for fuzzy control strategy, Phu et al. (2015) proposed an adaptive fuzzy controller and applied it to vibration control of a seat suspension system with an MREA. Later, Phu et al. (2017) proposed and realized an adaptive hybrid controller using sliding mode controller and H∞ control technique, which improved the control efficiency much in the profiles of random bump excitation, regular bump excitation, and random-step-wave excitation bump. Such hybrid controllers are a very inspiring method for dealing with different control objectives. Du et al. (2011) and Ning et al. (2018) proposed a semi-active seat suspension with MR elastomer for continuous stiffness adjustment and studied the corresponding control strategies for roll and vertical vibration caused by the heavy-duty vehicles on uneven roads. Sun et al. (2015) investigated a MR seat suspension system based on a MR elastomer isolator with negative stiffness and such controllability property is of help to achieve better ride comfort than passive seat suspension systems. Ning et al. (2016) designed and tested a scissor-type active seat suspension system using an electric motor. Meanwhile, a static output feedback H∞ controller with friction compensation capability is designed to achieve better ride comfort with relatively low costs.

In fact, the structural design and control strategy of the seat suspension systems aiming at vibration attenuation are not optimal for the objective of the shock control (Bai et al., 2017b). In the vibration control, the end-stop impact is not considered much in the structural design of the seat suspension systems, which means that the seat suspension travel stroke is not taken into account in the control strategies. As known, however, making full use of the EA stroke (i.e. the seat suspension travel stroke) will absorb impact energy as much as possible, which will be more likely to minimize the peak impact acceleration and time acting on the occupant's body (spine). Moreover, as compared to active seat suspension systems, ER/MR semi-active seat suspensions have shown their potentials in impact mitigation applications. ER/MR semi-active actuators could, after all, provide the performance of dissipating kinetic energy as passive actuators in case of failure of the control systems. Wu and Griffin (1997) utilized an EREA and on-off control strategy to reduce the possibility of end-stop impact, but the seat suspension travel stroke was not fully used and minimization of the deceleration was not the objective. To mitigate the biodynamic response to vibratory and blast-induced shock loads, Choi and Wereley (2005) designed a semi-active nonlinear optimal control algorithm for MR seat suspension. But it would be difficult to balance the vibration and shock control capabilities if only one control strategy is used.

The essential of "soft-landing" concept-based control systems using the EREAs/MREAs is the efficient usage of the EREA/MREA stroke and effective control of strong nonlinear hysteretic damping forces of the EREAs/MREAs. Wereley et al. (2011) analyzed non-dimensional stroke, velocity, and acceleration of the single-degree-of-freedom drop-induced shock mitigation systems and designed an optimal Bingham number control to minimize the shock loads transmitted to the payload by utilizing the maximal MREA stroke. Later, using MREA, Singh and Wereley (2014) minimized the recoil loads transmitted to the gun structure to maximize rate of fire.

To describe and track nonlinear hysteretic damping forces of MREAs, Weber (2013) proposed an approach that estimates the MREA damping forces by calculating in parallel several Bouc-Wen models with different constant excitation currents under given displacement and velocity excitations. The desired excitation current of the MREA can be determined by a piecewise linear interpolation scheme according to the desired and estimated damping forces. The accuracy for describing and predicting MREA damping force mainly depends on the hysteresis models. We previously proposed and validated an updated hysteresis model based on the phenomenological model (Bai et al., 2015), and later proposed and investigated a general hysteresis modeling approach featuring "shape function and memory mechanism" (Chen et al., 2018). The proposed resistor-capacitor (RC) operator was used to replace the Bouc-Wen operator to describe the nonlinear hysteresis characteristics, and the computational efficiency was

improved over 100% (Bai et al., 2019; Chen et al., 2018).

Based on the literature reviewed above, aiming at addressing the problems of the "impact effect" due to the blast-induced shock and the "discomfort" due to the undulation of terrain, semi-active seat suspension system with both vibration and shock mitigation performances and the function of switching control strategies in between vibration and shock according to the excitation and response is a topic worthy of study. Few literature could be found for referring so far. The main technical contribution of this study is as follows: (1) an MR semi-active seat suspension system for both vibration and shock mitigation is proposed and the dynamic model of the seat suspension system with a 4-degree-of-freedom lumped-parameter model for seated occupants is established; (2) a hybrid controller including a sky-hook control strategy to realize vibration attenuation, a "soft-landing" control strategy to achieve shock mitigation, and a method for switching the two control strategies according to the excitation and response of the seat are proposed; and (3) a feedforward tracking control strategy based on a hysteresis model with an RC operator is proposed to realize efficient control of the desired damping force of MREA.
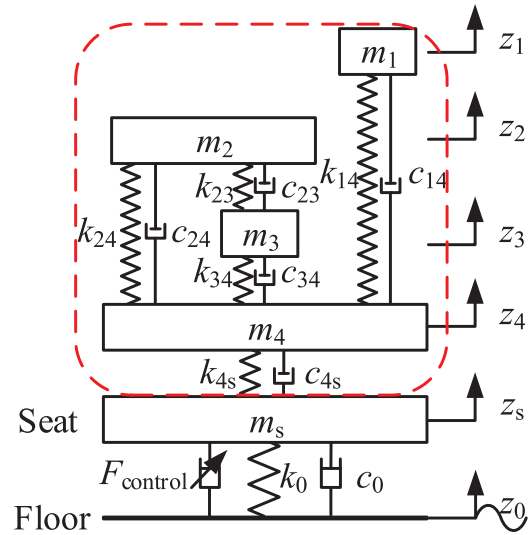
2. MR semi-active seat suspension system

In order to realize a seat suspension system with both vibration and shock mitigation capabilities for special vehicles, a semi-active seat suspension system using MREA is proposed and presented in Figure 1. The proposed semi-active seat suspension system consists of a coil spring supporting the seat and the occupant, an MREA as the main energy absorbing actuator, and a fail-safe EA rod. Kinetic energies of excitations, that is, vibration and shock, are dissipated by the MREA. The fail-safe EA rod collapses to dissipate the residual kinetic energy, if the MREA is unable to absorb all of them, which will minimize the impact damage on the human spine.

A dynamic model of the seat suspension system with a 4-degree-of-freedom lumped-parameter model for seated occupants, presented in Figure 2, is established to quantitatively evaluate the biodynamic response of the parts of the human body in vibration and shock mitigation. As shown in Figure 2, the dashed box is a 4-degree-of-freedom lumped-parameter model for the seated occupants (Bai et al., 2017c). The model consists of head, viscera, upper torso, and pelvis, with masses of m_1, m_2, m_3, and m_4 (i.e. m_i ($i = 1, 2, 3, 4$)), respectively. The stiffness of the two connected parts is k_{ij} ($i = 1, 2, 3, 4; j = 1, 2, 3, 4$) and the damping is c_{ij} ($i = 1, 2, 3, 4; j = 1, 2, 3, 4$). The state-space model of the proposed MR semi-active seat suspension system is
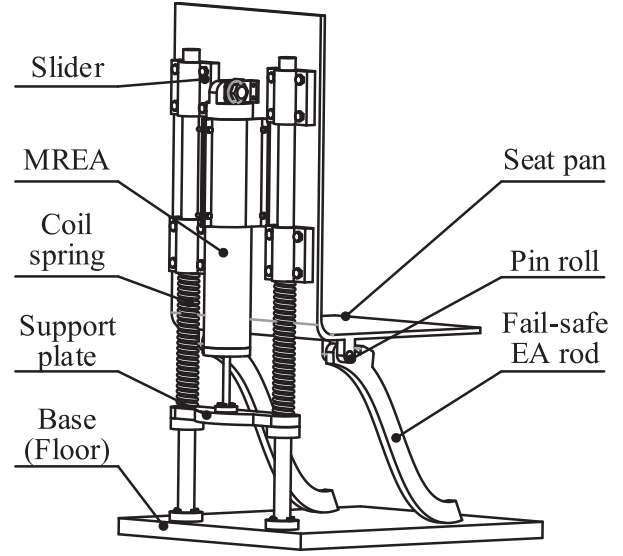
Figure 1. The MR seat suspension system for both shock and vibration mitigation.

Figure 2. Dynamic model of the MR seat suspension system with a seated occupant.

$$\begin{cases} \dot{X}(t) = \mathbf{A}X(t) + \mathbf{B}U(t) \\ Y(t) = \mathbf{C}X(t) + \mathbf{D}U(t) \end{cases} \qquad (1)$$

where state $X(t) = [\dot{z}_1 \quad \dot{z}_2 \quad \dot{z}_3 \quad \dot{z}_4 \quad \dot{z}_s \quad z_1 \quad z_2 \quad z_3 \quad z_4 \quad z_s]^T$, input $U(t) = [z_0 \quad \dot{z}_0 \quad F_{control}]^T$, and output $Y(t) = [\ddot{z}_1 \quad \ddot{z}_2 \quad \ddot{z}_3 \quad \ddot{z}_4 \quad \ddot{z}_s]^T$, $\mathbf{A} = \begin{bmatrix} \mathbf{A}_1 & \mathbf{A}_2 \\ \mathbf{A}_3 & \mathbf{A}_4 \end{bmatrix}$, $\mathbf{B} = \begin{bmatrix} \mathbf{B}_1 \\ \mathbf{B}_2 \end{bmatrix}$, $\mathbf{C} = [\mathbf{A}_1 \quad \mathbf{A}_2]$, and $\mathbf{D} = \mathbf{B}_1$. $\mathbf{A}_1$, $\mathbf{A}_2$, $\mathbf{A}_3$, $\mathbf{A}_4$, $\mathbf{B}_1$, and $\mathbf{B}_2$ are, respectively, given by
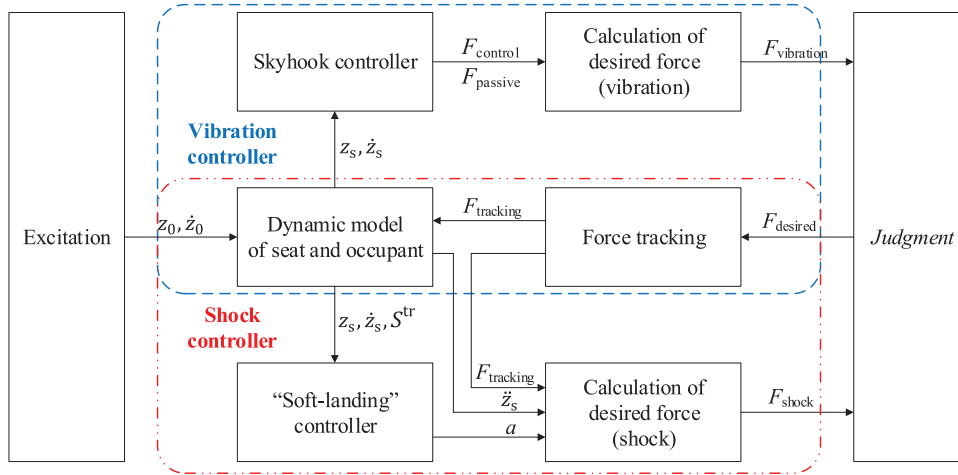
Figure 3. Schematic of the hybrid controller.

$$\mathbf{A}_1 = \begin{bmatrix} -\frac{c_{14}}{m_1} & 0 & 0 & \frac{c_{14}}{m_1} & 0 \\ 0 & -\frac{c_{23}+c_{24}}{m_2} & \frac{c_{23}}{m_2} & \frac{c_{24}}{m_2} & 0 \\ 0 & \frac{c_{23}}{m_3} & -\frac{c_{23}+c_{34}}{m_3} & \frac{c_{34}}{m_3} & 0 \\ \frac{c_{14}}{m_4} & \frac{c_{24}}{m_4} & \frac{c_{34}}{m_4} & -\frac{c_{14}+c_{24}+c_{34}+c_{4s}}{m_4} & \frac{c_{4s}}{m_4} \\ 0 & 0 & 0 & \frac{c_{4s}}{m_s} & -\frac{c_{4s}+c_0}{m_s} \end{bmatrix}$$

$$\mathbf{A}_2 = \begin{bmatrix} -\frac{k_{14}}{m_1} & 0 & 0 & \frac{k_{14}}{m_1} & 0 \\ 0 & -\frac{k_{23}+k_{24}}{m_2} & \frac{k_{23}}{m_2} & \frac{k_{24}}{m_2} & 0 \\ 0 & \frac{k_{23}}{m_3} & -\frac{k_{23}+k_{34}}{m_3} & \frac{k_{34}}{m_3} & 0 \\ \frac{k_{14}}{m_4} & \frac{k_{24}}{m_4} & \frac{k_{34}}{m_4} & -\frac{k_{14}+k_{24}+k_{34}+k_{4s}}{m_4} & \frac{k_{4s}}{m_4} \\ 0 & 0 & 0 & \frac{k_{4s}}{m_s} & -\frac{k_{4s}+k_0}{m_s} \end{bmatrix}$$

$$\mathbf{A}_3 = \mathrm{diag}(11111)$$

$$\mathbf{A}_4 = \mathrm{zeros}(5,5), \quad \mathbf{B}_1 = \begin{bmatrix} 0 & 0 & 0 \\ 0 & 0 & 0 \\ 0 & 0 & 0 \\ 0 & 0 & 0 \\ \frac{k_0}{m_s} & \frac{c_0}{m_s} & -\frac{1}{m_s} \end{bmatrix}, \quad \mathbf{B}_2 = \mathrm{zeros}(5,3)$$

where m_s is the seat mass; k_{4s} and c_{4s} are the stiffness and the damping between the seat and the pelvis, respectively; k_0 is the stiffness of the coil spring; c_0 is the passive damping of the MREA; F_{control} is the controllable damping force provided by the MREA; z_0 is the displacement excitation; $z_i (i = 1, 2, 3, 4, s)$ is the displacement responses (of the head, the viscera, the upper torso, the pelvis, and the seat); and $\dot{z}_i (i = 1, 2, 3, 4, s)$ and $\ddot{z}_i (i = 1, 2, 3, 4, s)$ are the corresponding velocity and acceleration responses, respectively.

3. Hybrid controller design

3.1. Vibration controller

Figure 3 presents the schematic of the hybrid controller for both vibration and shock mitigation with a common employment of the model of seated occupant and force tracking mechanism. The hybrid controller consists of a vibration controller, a shock controller, and a *Judgment* unit. The hybrid controller will switch control in between the two sub-controllers after the *Judgment* evaluation. As shown in Figure 3, the dashed box is the schematic of the vibration controller. The skyhook control strategy (Karnopp et al., 1974) is employed for the vibration control. According to velocity excitations and seat velocity responses, the controllable damping force can be obtained by the skyhook control strategy. The desired damping force of the vibration control is composed of controllable damping force controlled by the skyhook controller and passive damping force of the MREA. In the state of vibration control, the desired damping force is the output of the hybrid controller. The force tracking unit outputs tracking damping force following the desired damping force. Since the responses of the human body are difficult to obtain in practical applications, the seat response is used as the control target. The skyhook control strategy is expressed as

$$F_{\mathrm{control}} = \begin{cases} C_{\mathrm{sky}}\dot{z}_s & \dot{z}_s(\dot{z}_s - \dot{z}_0) \geqslant 0 \\ 0 & \dot{z}_s(\dot{z}_s - \dot{z}_0) < 0 \end{cases} \quad (2a)$$

$$F_{\mathrm{desired}} = F_{\mathrm{vibration}} = F_{\mathrm{control}} + F_{\mathrm{passive}} \quad (2b)$$

where C_{sky} is the skyhook damping; F_{control} is the controllable damping force controlled by the skyhook controller; F_{passive} is the passive damping force of the MREA; and $F_{\mathrm{vibration}}$ is the desired damping force from the vibration controller, which is the sum of the controllable damping force and the passive damping force of the MREA. The desired damping force of the hybrid controller is equal to that of the vibration controller when only in vibration control, as shown in the dashed box in Figure 3.

3.2. Shock controller

For the purpose of protecting the occupants as much as possible, the shock controller based on the concept
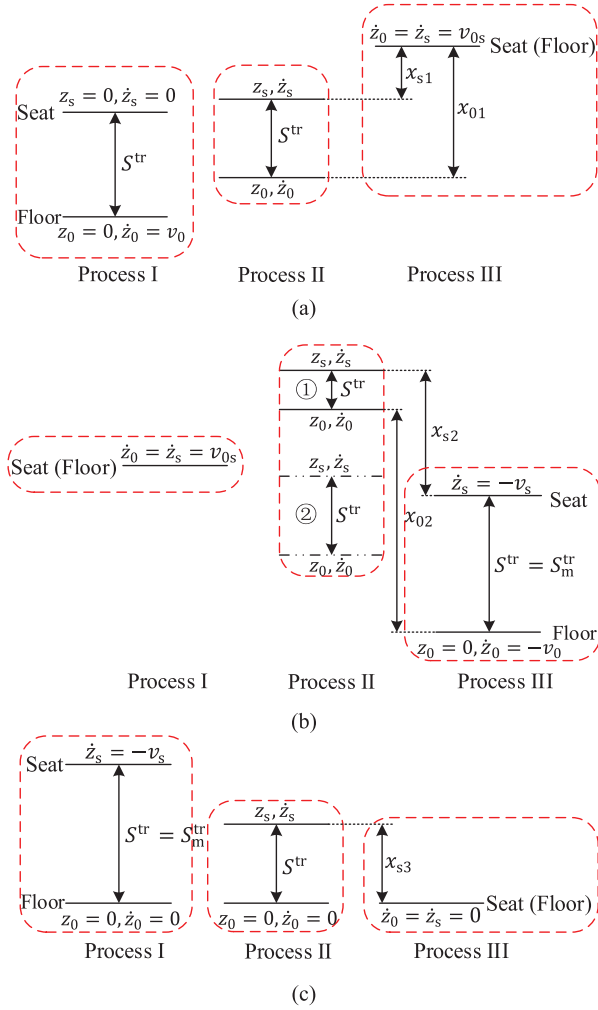
Figure 4. Decomposition of the seat motion process under blast-induced shock excitation under "soft-landing" control: (a) the seat suspension compression, (b) the seat suspension rebound, and (c) the second compression of the seat suspension.

of "soft-landing" (Wereley et al., 2011) is utilized for the shock excitation. In detail, as shown in Figure 3, the shock control based on the "soft-landing" concept is to accurately calculate the desired damping force of the employed MREA, ensuring that the seat suspension travel stroke could be fully utilized and the seat decelerates at a constant deceleration. Minimized shock damage (i.e. the deceleration) to the seated occupants is expected.

The shock process of a special vehicle subjected to blast is taken as an example for shock control in this study. The shock process can be decomposed into three phases under "soft-landing" goal-based control. Figure 4(a) to (c) presents the motion of the seat suspension compression, rebound, and second compression after a blast-induced shock excitation, respectively. The horizontal lines in Figure 4 indicate the positions of the vehicle floor (the excitation) and the seat (the response). The vertical gap between vehicle floor and the seat is the MREA travel stroke.

Figure 4(a) is the first phase, seat suspension compression process: process I is a shock acting on the vehicle floor, then the vehicle instantaneously gets a velocity $\dot{z}_0 = v_0$ and the start displacement is $z_0 = 0$. In process II, the vehicle floor moves up at a velocity $\dot{z}_0$, pushing the seat up and compressing the seat suspension. Then, the vehicle floor is decelerated by gravity and the seat is accelerated at a desired acceleration controlled by the shock controller with the desired damping force output. In process III, both the vehicle floor and the seat velocities are the same (i.e. $\dot{z}_0 = \dot{z}_s = v_{0s}$), so the seat suspension is no longer compressed. In the first phase of "soft-landing," the seat suspension is compressed to the bottom, making full use of the seat suspension travel stroke.

Figure 4(b) is the second phase, seat suspension rebound process: process I follows the end of the process III of the first phase, and the vehicle floor and the seat move with the same velocity (i.e. $\dot{z}_0 = \dot{z}_s = v_{0s}$) initially. Two possible cases for process II: if $v_{0s} > 0$, the vehicle floor and the seat rise first (i.e. the state ①), then the two drop together (i.e. the state ②); if $v_{0s} = 0$, the two descend together to the state ② directly. For the propose of keeping the seat suspension rebounded, regardless of the state ① or ②, it is necessary to control the desired damping force so that the deceleration of the seat is less than the gravitational acceleration of the floor. In process III, the floor velocity reaches $-v_0$, which is numerically equal to that of the process I of the first phase shown in Figure 4(a). The floor is blown upward when the floor velocity is numerically equal to v_0, which indicates the floor is about to drop to the ground and then the velocity dips to 0. At this point, the seat suspension travel stroke should be rebounded to the maximum $S^{tr} = S_m^{tr}$, which is ready for the second impact of the third phase, providing the maximal compressible seat suspension travel stroke. The seat velocity is $\dot{z}_s = -v_s$.

Figure 4(c) is the third phase, seat suspension second compression process: in process I, the floor impact onto the ground, then its velocity suddenly drops to 0 and the seat starts to accelerate with the velocity $-v_s$. In process II, the seat suspension continues to compress and seat accelerates at the desired acceleration controlled by the shock controller. In process III, the seat accelerates at the desired acceleration until the velocity reaches 0, and at this time, the seat suspension is just compressed to the bottom and full seat suspension travel stroke has been consumed. It is noted that the variables discussed in this study are all positive in the vertical upward.

The shock controller, that is, "soft-landing" controller, as shown in dash-dotted box in Figure 3, calculates the expected acceleration a according to the system state. Then, the desired damping force F_{shock} of the shock controller is obtained based on the current acceleration of the system and the feedback of the force

tracking system. The desired damping force of hybrid controller is equal to that of the shock controller when under pure shock conditions. The desired acceleration can be calculated based on the motion decomposition of the shock process shown above in Figure 4. According to Figure 4(a), the desired acceleration of the first phase can be calculated and expressed as

$$2gx_{01} = v_{0s}^2 - \dot{z}_0^2 \qquad (3a)$$

$$2ax_{s1} = v_{0s}^2 - \dot{z}_s^2 \qquad (3b)$$

$$x_{01} = x_{s1} + S^{tr} \qquad (3c)$$

$$a = g(v_{0s} - \dot{z}_s)/(v_{0s} - \dot{z}_0) \qquad (3d)$$

where a is the desired acceleration; g is the gravity; S^{tr} is the rest seat suspension travel stroke; v_{0s} is the common velocity of both the floor and the seat when the seat suspension is compressed to the bottom; x_{01} is the motion displacement of the floor at any time in the first phase decelerating from the velocity $\dot{z}_0$ to the velocity v_{0s}; and x_{s1} is the motion displacement of the seat at any time in the first phase accelerating from the velocity $\dot{z}_s$ to the velocity v_{0s}.

According to Figure 4(b), the desired acceleration of the second phase can be calculated and expressed as

$$2gx_{02} = v_0^2 - \dot{z}_0^2 \qquad (4a)$$

$$2ax_{s2} = v_s^2 - \dot{z}_s^2 \qquad (4b)$$

$$x_{s2} = x_{02} + S_m^{tr} - S^{tr} \qquad (4c)$$

$$a = g(v_s - \dot{z}_s)/(v_0 - \dot{z}_0) \qquad (4d)$$

where S_m^{tr} is the total seat suspension travel stroke; x_{02} is the motion displacement of the floor at any time in the second phase decelerating from the velocity $\dot{z}_0$ to the velocity $-v_0$; x_{s2} is the motion displacement of the seat at any time in the second phase decelerating from the velocity $\dot{z}_s$ to the velocity $-v_s$.

According to Figure 4(c), the desired acceleration of the third phase can be calculated and expressed as

$$2ax_{s3} = 0^2 - \dot{z}_s^2 \qquad (5a)$$

$$x_{s3} = -S^{tr} \qquad (5b)$$

where x_{s3} is a motion displacement of the seat at any time in the third phase accelerating from the velocity $\dot{z}_s$ to the velocity 0.

Then the desired damping force can be obtained according to the desired acceleration of each phase and is given by

$$\Delta + m_s a = m_s \ddot{z}_s \qquad (6a)$$

$$F_{desired} = F_{shock} = F_{tracking} + \Delta \qquad (6b)$$

where $m_s a$ is the resultant external force required to reach the desired acceleration a; $m_s \ddot{z}_s$ is the resultant

external force at this time; Δ is the difference of the resultant external force between the desired acceleration a and the actual acceleration $\ddot{z}_s$.

The proposed shock control strategy in this study has at least three particular advantages: (1) the desired damping force can be adjusted itself based on the mass of the seated occupants; (2) the desired damping force can be updated in real time based on the system states; and (3) error between the tracking damping force and the desired damping force can be compensated in real time.

3.3. Judgment for switching control strategies under hybrid excitations

It is critical to switch the hybrid controller to the vibration controller or the shock controller, since the control objective and the corresponding performance of the vibration and the shock controllers are different. However, both vibration and shock to the system are unknown. The difference between the vibration and shock is even less known. The essential of the *Judgment* for switching control strategies is to evaluate the occurrence of end-stop impact. The reason for occurrence of end-stop impact is that the velocities of the excitation and seat response are never equal in the entire MREA stroke. Based on the current system state, such as the excitation velocity, the MREA's stroke, and possible maximal output damping force of the MREA, end-stop impact occurrence can be calculated or predicted. The hybrid controller enters the state of shock control when is judged as "shock," otherwise it stays in the state of vibration control.
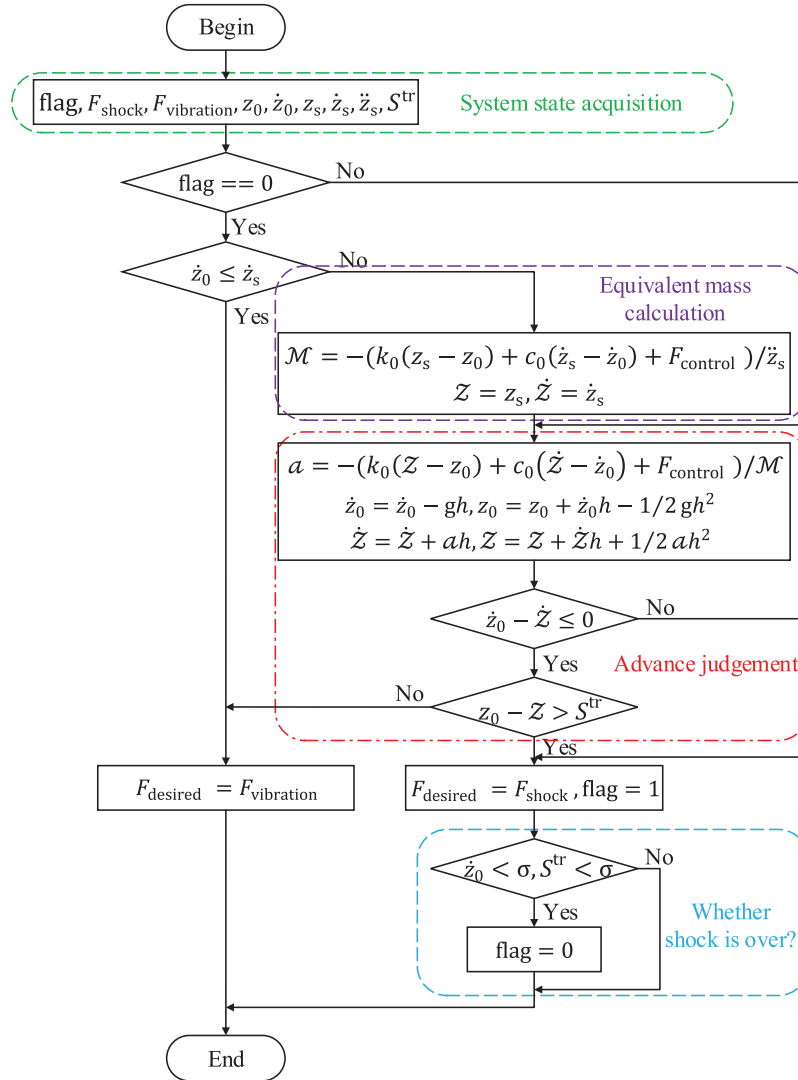
The flow chart of the *Judgment* of the hybrid controller shown in Figure 3 is presented in Figure 5. As shown in Figure 5, it consists of four parts. The first part is the system state acquisition, including the displacements and velocities of the excitation and the seat and the rest seat suspension travel stroke. Static variable "flag" is set to "0" initially. The variable is used to determine the current system state, "0" indicates vibration control state and "1" indicates shock control state.

The second part is the equivalent mass calculation. In practical applications, it is difficult to get real-time status of the parts of the seated occupant. The seated occupant and the seat is assumed to be a whole entity. According to the current system state, an equivalent mass can be calculated, and the dynamic model of MR semi-active seat suspension system with an equivalent mass can be expressed as

$$k_0(z_s - z_0) + c_0(\dot{z}_s - \dot{z}_0) + F_{control} + \mathcal{M}\ddot{z}_s = 0 \qquad (7)$$

where $\mathcal{M}$ is the equivalent mass. The equivalent mass is calculated only under a condition that an excitation velocity is greater than the response velocity. Then, the

Figure 5. Flow chart of the *Judgment* of the hybrid controller.

displacement and the velocity of the equivalent mass at the current moment can be expressed as

$$\mathcal{Z} = z_s, \ \dot{\mathcal{Z}} = \dot{z}_s \qquad (8)$$

where $\mathcal{Z}$ and $\dot{\mathcal{Z}}$ are the displacement and the velocity of the equivalent mass. The equivalent mass is calculated via equation (7), so the displacement and the velocity of the equivalent mass are equal to the displacement and the velocity of the seat at this moment.

The third part is the advance judgment of end-stop impact occurrence. The triggering of shock control is only considered in the case that excitation velocity is greater than the response velocity. So the reason for the end-stop impact is that excitation velocity is always greater than the response velocity in the range of the seat suspension travel stroke. As shown in the dash-dotted box in Figure 5, it continues cycling until the excitation velocity is not greater than the response

velocity and then exits the cycle. The seat suspension travel stroke required for the cycle is compared to the rest seat suspension travel stroke at the current system. If the former is greater than the latter, the end-stop impact would occur in condition of vibration control. Therefore, the shock control should be conducted. Otherwise, the system stays in vibration control. When the system enters the shock control, the variable "flag" is set to be "1."

The fourth part is to judge whether the shock control is over. When the seat velocity is 0 and the seat suspension travel stroke is used up, the shock control ends. The variable "flag" is set to "0." σ shown in Figure 5 is a preset constant ($\sigma = 0.001$ in this study).

It should be noted that only when the excitation velocity is greater than the response velocity, the shock control is considered, that is, the type of excitation is large road obstacle or explosion impact. Moreover, once the hybrid controller enters the shock control
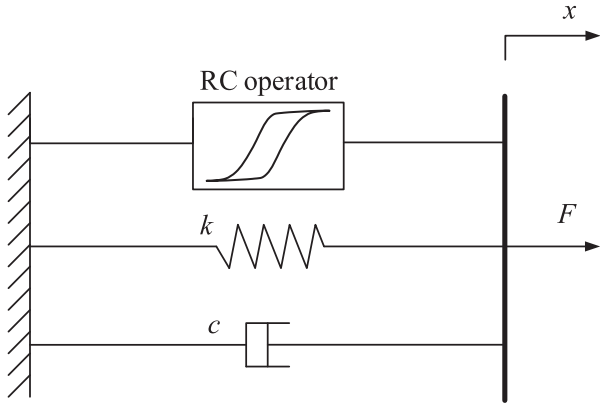
Figure 6. Schematic of the basic RC operator–based hysteresis model.

state, the entire process of shock control must be completed before jump out. The proposed hybrid controller could also work for the case of a big hole on the road, if the distance between the vehicle floor and the road can be detected.

4. Basic RC operator–based hysteresis model and force tracking for MREAs

4.1. Hysteresis modeling

The RC operator (Bai et al., 2019; Chen et al., 2018) is a hysteresis operator proposed by Bai's group as the kernel of the hysteresis models to describe/predict the hysteretic nonlinearities. Figure 6 shows the schematic of the basic RC operator–based model for nonlinear hysteresis of MREAs with the RC operator replacing the Bouc-Wen operator (Wen, 1976). The damping force of MREA can be expressed as

$$F = c\dot{x} + \alpha z + kx + f \tag{9}$$

$$z(t) = 1 - 2e^{-g_1(S)/p}, \text{ when } \dot{x}(t) > 0 \tag{10a}$$

$$z(t) = -1 + 2e^{g_2(S)/p}, \text{ when } \dot{x}(t) < 0 \tag{10b}$$

$$\dot{z}(t) = 0, \text{ when } \dot{x}(t) = 0 \tag{10c}$$

$$S_0 = g_1^{-1}(-\ln((1 - z(t^*))/2)p), x_0 = x(t^*), \\ \text{when uploading} \tag{10d}$$

$$S_0 = g_2^{-1}(\ln((1 + z(t^*))/2)p), \\ x_0 = x(t^*), \text{ when downloading} \tag{10e}$$

$$S(t) = S_0 + x(t) - x_0 \tag{10f}$$

$$g_1(S) = |S|^q \tag{10g}$$

$$g_2(S) = -|S|^q \tag{10h}$$

where F is the damping force of MREA; f is the elastic force at the initial displacement; c, α, and k are the damping, the hysteresis, and the stiffness, respectively; x, $\dot{x}$, and z are the displacement excitation, the velocity excitation, and the hysteresis output, respectively; the range of the hysteresis output z value is $(-1,1)$, which is normalized as equation (10a) to (10c); p is a hysteresis factor and $p > 0$; S is a virtual displacement variable; the shape functions $g_1(S)$ and $g_2(S)$ are the monotonic functions; $g_1(S)^{-1}$ and $g_2(S)^{-1}$ are the inverse functions of $g_1(S)$ and $g_2(S)$, respectively; q is a time-varying hysteresis factor; S_0 and x_0 are the virtual displacement reference point and displacement reference point at the moment t^* when under the new monotone excitation, respectively.

4.2. Force tracking principle

Figure 7 presents the schematic of the feedforward force tracking using the basic RC operator–based hysteresis model. The force tracking principle is expressed as

$$F_{\text{tracking}} = c\dot{x} + \alpha\hat{z} + kx + f \tag{11a}$$

$$F_{\text{desired}} = \lambda\dot{x} \tag{11b}$$

$$c = c_1 I^2 + c_2 I + c_3 \tag{11c}$$

$$\alpha = \alpha_1 I^2 + \alpha_2 I + \alpha_3 \tag{11d}$$

$$\min(|F_{\text{tracking}} - F_{\text{desired}}|), I \in [0, I_{\max}] \tag{11e}$$

where F_{tracking} is the tracking force; F_{desired} is a desired damping force, which is given by the velocity excitation multiplied the desired damping λ; c and α are the parameters related to the excitation current I; and the parameters c_1, c_2, c_3 and α_1, α_2, α_3, respectively, fit the relationship between c, α, and I, which are fitted using equations (11c) and (11d). The hysteresis output $\hat{z}$ is obtained by equations (10a) to (10h). Equation (11e) can be expanded as
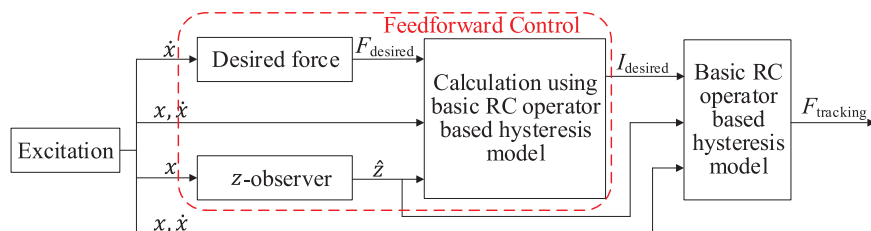
Figure 7. Schematic of the force tracking using the basic RC operator–based hysteresis model.
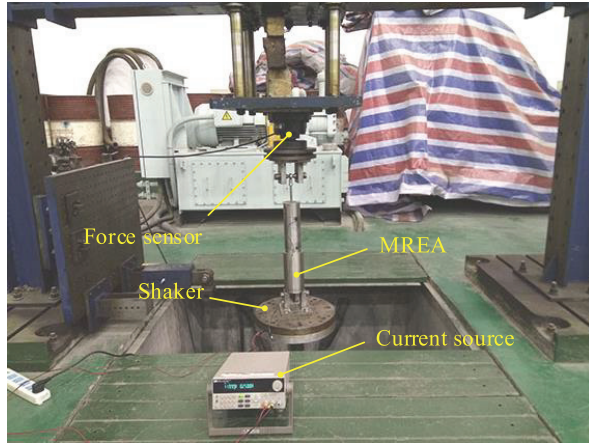
Figure 8. The self-developed MREA prototype in the experimental setup.

$$\min\left(\left|\mathrm{E}I^2 + \mathrm{L}I + \mathrm{N}\right|\right), I \in [0, I_{max}] \qquad (12)$$

where $\mathrm{E}(= c_1\dot{x} + \alpha_1\hat{z})$, $\mathrm{L}(= c_2\dot{x} + \alpha_2\hat{z})$, and $\mathrm{N}(= (c_3 - \lambda)\dot{x} + \alpha_3\hat{z} + kx + f)$ are the variables that are independent of excitation current and are only

related to the external excitation. In other words, the problem of finding a desired excitation current can be transformed into the optimal solution problem of the quadratic function.
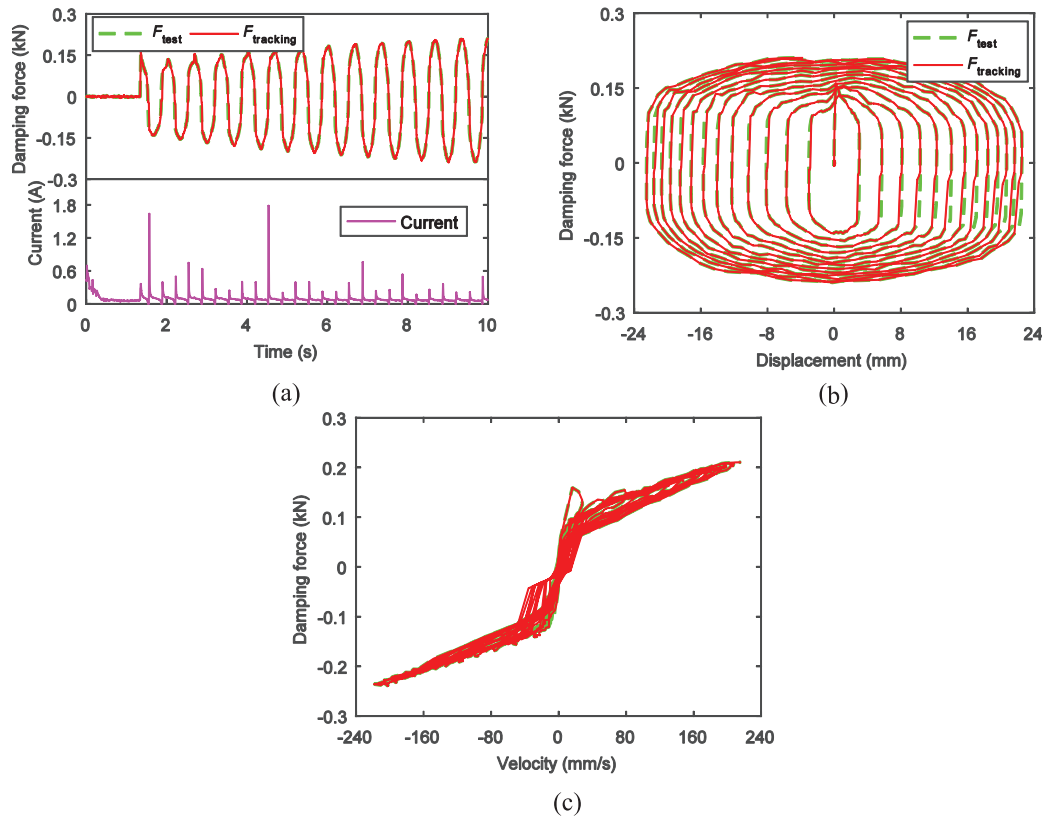
4.3. Force tracking performance

A self-developed MREA prototype for the proposed MR semi-active seat suspension system in the experimental setup is shown in Figure 8. Sinusoidal displacement excitations are provided by a servo hydraulic test rig (Type: LFH-LFV3068, SAGINOMIYA Inc.). The MREA is tested and the 10 parameters ($p, q, c_1, c_2, c_3, \alpha_1, \alpha_2, \alpha_3, k$, and f) are identified using the genetic algorithm and the experimental data. The simulation of the system shown in Figure 7 is made in MATLAB/Simulink using solver ode3 (Bogacki-Shampine) with a fixed time step size of 0.0001 s. The input to MATLAB/Simulink model is a sinusoidal displacement excitation with an amplitude of 30 mm and a frequency of 2 Hz.

Figure 9(a) to (c) presents the time histories of the damping force and the excitation current, the tracking trajectories of the damping force versus displacement, and the tracking trajectories of the damping force
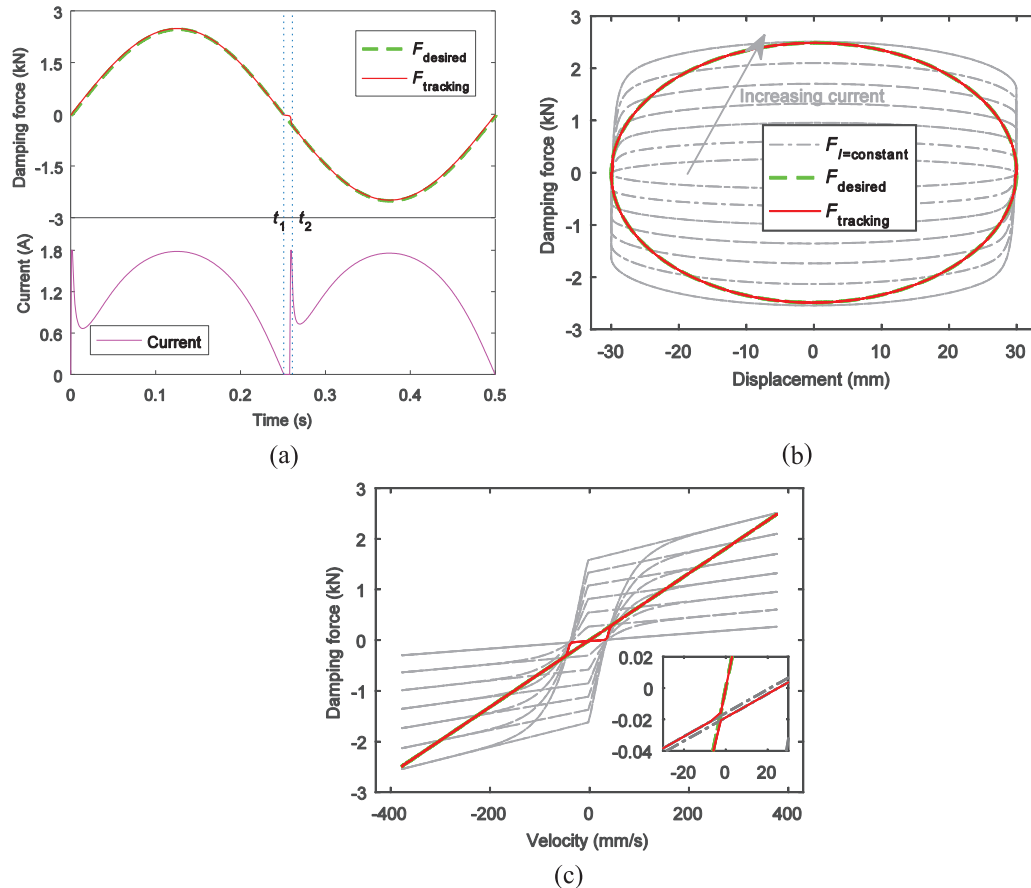
Figure 9. Simulated results of the force tracking performance: (a) the time histories of the damping force and the excitation current, (b) the tracking trajectories of the damping force versus displacement, and (c) the tracking trajectories of the damping force versus velocity.

Figure 10. Force tracking performance when the MREA prototype is under a sinusoidal displacement excitation with a maximal amplitude of 30 mm and a frequency of 1.5 Hz: (a) the time history of the damping force and the excitation current, (b) the tracking trajectories of the damping force versus displacement, and (c) the tracking trajectories of the damping force versus velocity.

versus velocity, respectively. The gray lines in Figure 9(b) and (c) are the simulated damping force of the MREA at different constant excitation currents (0–1.8 A, with an interval 0.3 A). As shown in Figure 9(a), comparing the time histories of the tracking damping force with the desired damping force, the tracking of the desired damping force can be efficiently achieved based on the principle shown in Figure 7. At the beginning, the excitation current reaches the maximum to fast track the desired damping force. At the time t_1–t_2, affected by the residual damping force and the pre-yield stiffness, even the excitation current drops to 0 A, the tracking error inevitably occurs. Combining with Figure 9(b) and (c), the trajectory of the tracking damping force is along with the minimum force versus velocity when the desired damping force is not greater than the passive damping force of the MREA. The tracking error has been minimized in all cases where feedback control is not used to minimize errors.
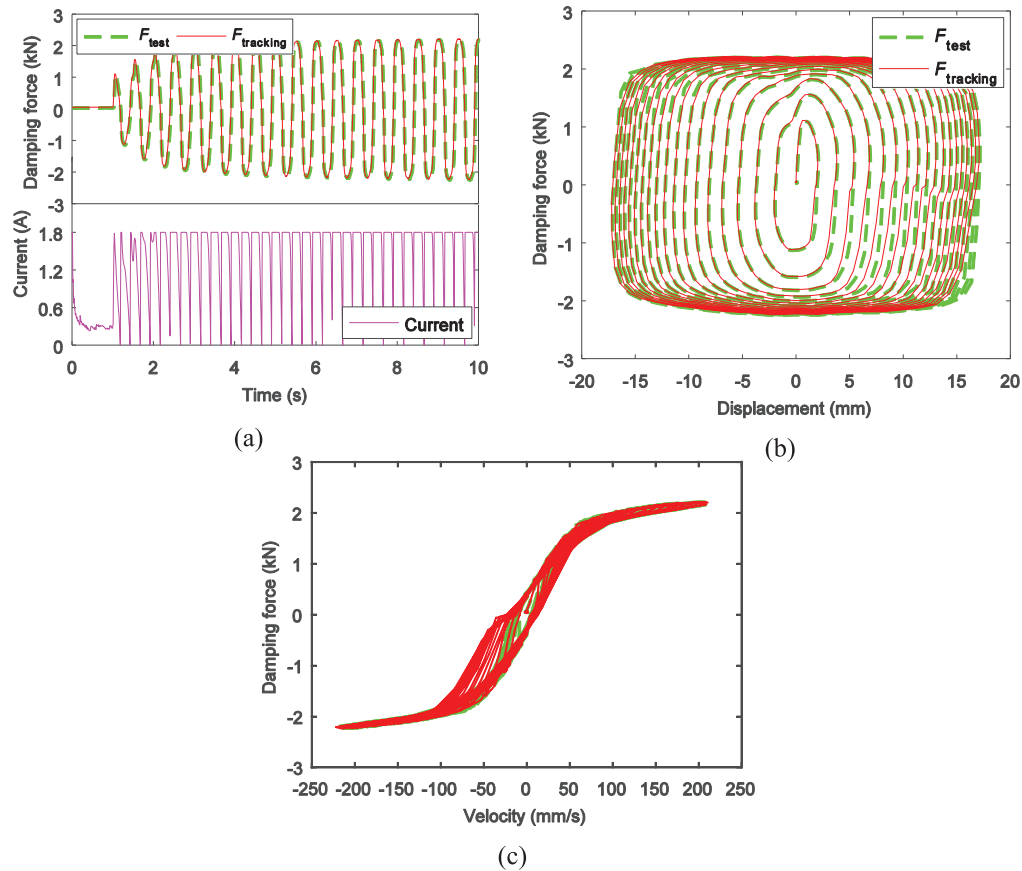
Figure 10(a) to (c) shows the time histories of the damping force and the excitation current, the tracking trajectories of the damping force versus displacement, and the tracking trajectories of the damping force versus velocity, when the MREA prototype is under a sinusoidal displacement excitation with a maximal amplitude of 30 mm and a frequency of 1.5 Hz,

respectively. F_{test} is the experimental data when excitation current is 0 A. As shown in Figure 9, $F_{tracking}$ can track F_{test} very well and the excitation current is almost equal to 0. Similarly, Figure 11(a) to (c) shows the time histories of the damping force and the excitation current, the tracking trajectories of the damping force versus displacement, and the tracking trajectories of the damping force versus velocity, when the MREA prototype is under a sinusoidal displacement excitation with a maximal amplitude of 20 mm and a frequency of 2 Hz, respectively. F_{test} is the acquired data with the MREA input excitation current equal to 1.8 A. As can be seen from Figure 11, the excitation current is basically around 1.8 A and $F_{tracking}$ tracks F_{test} very well.

5. Simulation and analysis

5.1. Vibration control

The skyhook damping is set to 1200 N s/m and the parameters of the seat suspension system are listed in Table 1. The vibration control system shown in the dashed box of Figure 3 is built in MATLAB/Simulink. The input to the system is a sinusoidal displacement with a 15 mm amplitude and frequencies from 0 to 20 Hz.

Figure 11. Force tracking performance when the MREA prototype is under a sinusoidal displacement excitation with a maximal amplitude of 20 mm and a frequency of 2 Hz: (a) the time history of the damping force and the excitation current, (b) the tracking trajectories of the damping force versus displacement, and (c) the tracking trajectories of the damping force versus velocity.

Figure 12(a) to (d) presents the transmissibility of the head, the viscera, the upper torso, and the pelvis of a seated occupant to the excitation from the floor, respectively. The passive state and passive-on state is realized with 0 and 1 A excitation currents in the MREA. As shown in Figure 12, at the resonance frequency of 2.6 Hz, the transmissibility of the passive state is the biggest. At this time, the vibration system does not attenuate vibration, but amplifies the excitation. At the passive-on state, that is, 1 A constant excitation current, the resonance frequency moves to around 4 Hz and it is close to the sensitive frequency of the human body. Comparing with the passive state and the passive-on state, the vibration attenuation performance with the skyhook controller is much better in both resonance region and isolation region. The resonance frequency is around 2.6 Hz, which indicates the sensitive frequency range of the human body just falls in the isolation region of the seat suspension system, maximizing the isolation of the system.

5.2. Shock control

The velocity of the floor is assumed to increase suddenly to 2 m/s after detonation of exploders. The total seat suspension travel stroke is 80 mm and the seat suspension equilibrium position is at the rest seat suspension travel stroke 50 mm in this study. The shock controller shown in the red dashed box of Figure 3 is built in MATLAB/Simulink using solver ode3 (Bogacki-Shampine) with a fixed time step size of 0.0001 s.

Figure 13(a) to (c) shows the time histories of the excitation velocity, the response velocity, the acceleration and the seat suspension travel stroke, the time histories of the damping force and the excitation current, and the time histories of the accelerations of each part of seated occupant, when under the shock excitation. As shown in Figure 13(a), the floor gets a velocity at the moment of detonation of exploders, then the floor moves up until impacting onto the ground. At this time, the velocity of floor suddenly drops to 0. The shock controller controls the output of the controllable damping force to slowly increase the seat velocity to v_{0s}. It is the seat suspension compression of the first phase. Then, the seat velocity is slightly bigger than the floor velocity, which is the seat suspension rebound of the second phase. Finally, the floor hits the ground, then seat suspension compresses again, which is the third phase. However, the shock controller controls the seat

**Table 1.** Parameters of the MR semi-active seat suspension system.

| Quantity	Symbol	Value	Units
Mass of head	m_1	6.142	kg
Mass of viscera	m_2	8.578	kg
Mass of upper torso	m_3	20.59	kg
Mass of pelvis	m_4	17.79	kg
Mass of seat	m_s	35	kg
Damping between head and pelvis	c_{14}	949.7	N s/m
Damping between viscera and upper torso	c_{23}	1851	N s/m
Damping between viscera and pelvis	c_{24}	861.9	N s/m
Damping between upper torso and pelvis	c_{34}	845.6	N s/m
Damping between pelvis and seat	c_{4s}	2358	N s/m
Damping of MREA at passive state	c_0	749	N s/m
Stiffness between head and pelvis	k_{14}	59,190	N/m
Stiffness between viscera and upper torso	k_{23}	22,740	N/m
Stiffness between viscera and pelvis	k_{24}	22,280	N/m
Stiffness between upper torso and pelvis	k_{34}	20,410	N/m
Stiffness between pelvis and seat	k_{4s}	92,750	N/m
Stiffness of coil spring	k_0	28,779	N/m

MR: magnetorheological; MREA: magnetorheological energy absorber.

velocity slowly to reduce to 0. As also seen from the time histories of the seat acceleration and the seat suspension travel stroke in Figure 13(a), the first phase is at the time 0–t_a, and the seat suspension is compressed. The seat and the floor velocities together reach v_{0s}, at which point the seat suspension travel stroke is used up. The second phase is at the time $t_a - t_b$, and the seat suspension is rebounded. When the time t_b is reached, the rest travel stroke of the seat suspension rebounds to the maximum of 80 mm. So the maximum seat suspension travel stroke is prepared for the second shock of the third phase. After the time t_b is the third phase, the second shock process, the seat suspension is compressed again. It can be seen from the acceleration curve in Figure 13(a) that the accelerations of the three phases is basically a constant acceleration. Fluctuations of the curves are caused by the track error of the desired damping force. In general, the control target of "soft-landing" can be achieved.

As presented in Figure 13(b), the MREA can output damping force along the desired damping force trajectory, indicating that the actuator can basically meet the performance requirements. It can also be seen from Figure 13(c) that the accelerations of each part of seated occupant change smoothly, which achieves the target of shock control, that is, "soft landing."

In order to highlight the advantages of the shock controller under the shock excitation, Figure 14
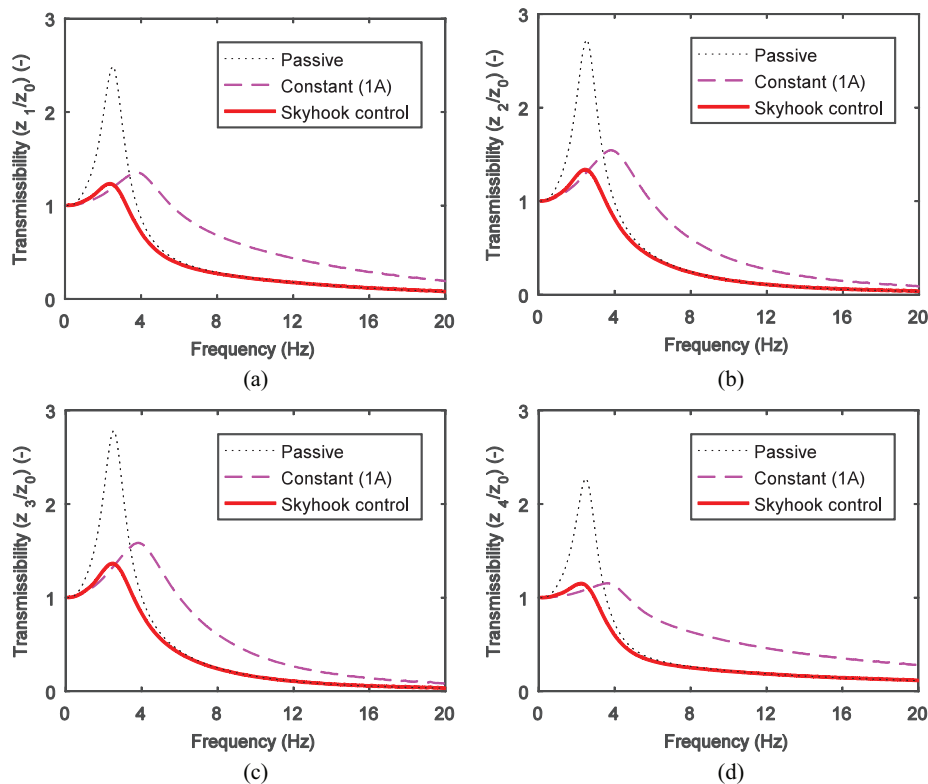
Figure 12. Transmissibilities of each part of the seated occupant on the proposed MR seat suspension system using vibration controller: (a) the head, (b) the viscera, (c) the upper torso, and (d) the pelvis.
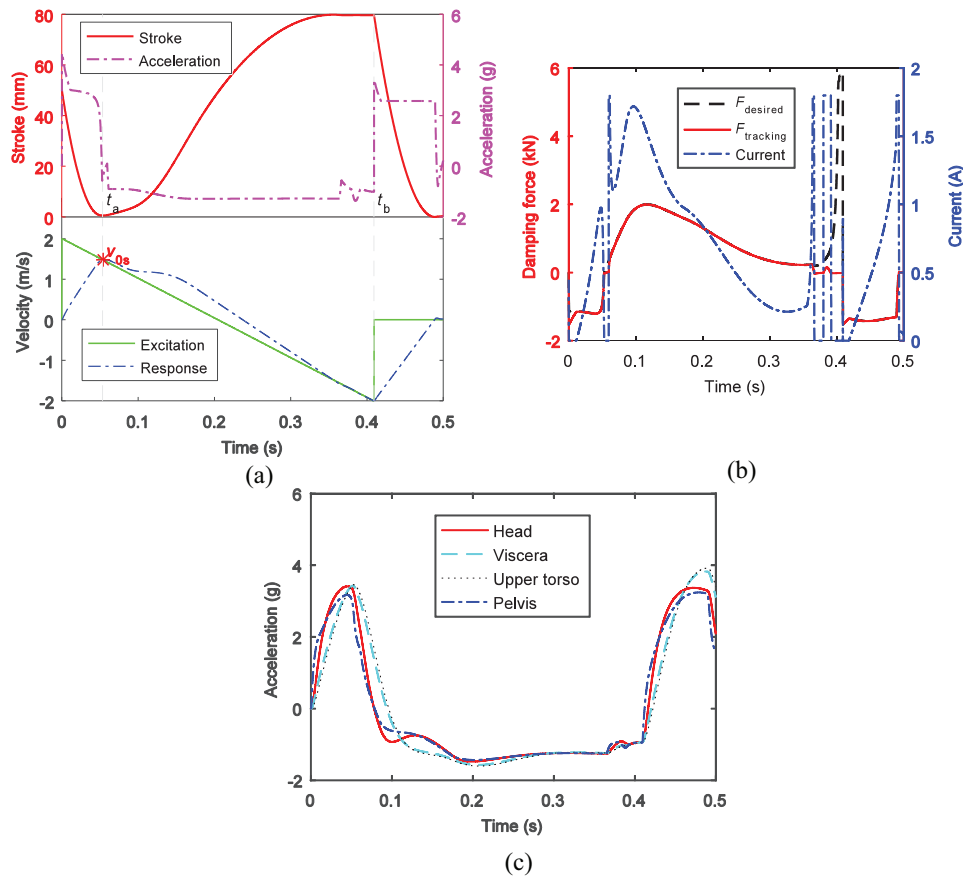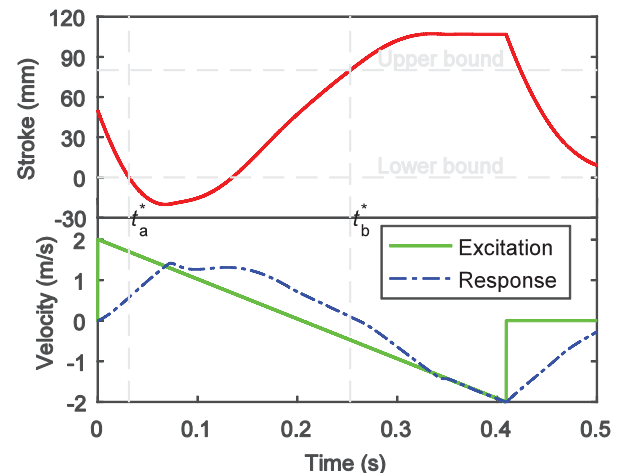
Figure 13. Shock mitigation performance using shock controller: (a) the time histories of the excitation velocity, the response velocity, the acceleration, and the seat suspension travel stroke; (b) the time histories of the damping force and the excitation current; and (c) the time histories of the accelerations of each part of seated occupant.

presents shock mitigation performance using the vibration controller, that is, skyhook control strategy. Comparing with Figure 13(a), the seat response velocity and the rest seat suspension travel stroke are totally different. At the time t_a^*, the seat suspension travel stroke has been used up, but the excitation velocity is still greater than that of the seat. Then the travel stroke shows negative values, which inevitably causes end-stop impact and discomfort even damages will occur to the seated occupants. At the time t_b^*, the seat suspension is rebounded to the maximal stroke of 80 mm. But the seat suspension is continuously rebounding. The reason is that the desired damping force given by the vibration controller is not sufficient. It is impossible in actual situations, which also causes end-stop impact. The compassion of Figures 13(a) and 14 further verifies that vibration controller and shock controller should be working cooperatively to achieve an optimal control objective for complex shock and vibration excitations.
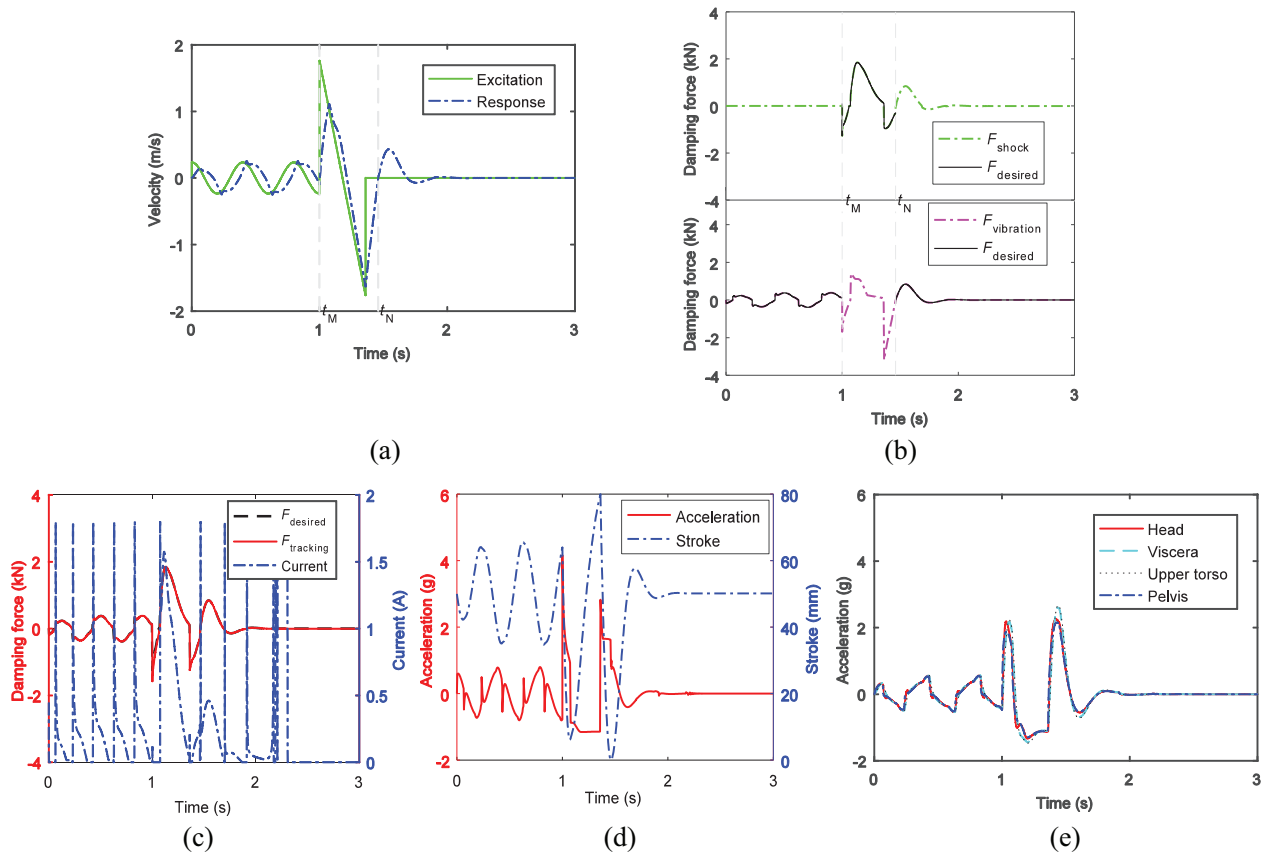
5.3. Hybrid control

Figure 15(a) to (e) shows the time histories of the excitation velocity and the response velocity, the desired

Figure 14. Shock mitigation performance using the vibration controller.

damping force of the hybrid controller, the damping force and the excitation current of the MREA, the seat suspension travel stroke and the seat acceleration, and each part acceleration of the seated occupant,

Figure 15. Time histories of the mitigation performance using the hybrid controller: (a) the excitation velocity and the response velocity, (b) the desired damping force of the hybrid controller, (c) the damping force and the excitation current of the MREA, (d) the seat suspension travel stroke and the seat acceleration, and (e) each part acceleration of the seated occupant.

respectively. As shown in Figure 15(a), the excitation consists of two parts. The first part is a sinusoidal displacement excitation with an amplitude of 15 mm and a frequency of 2.5 Hz during the time 0–1 s, and the second part is a shock excitation from the moment of 1.0001 s. In the process of shock control, there are two abrupt changes in the floor velocity, as analyzed before in Figure 4. One occurs at the moment of shock, and the other is when the floor falls back to the ground. Comparing with the floor velocity, the seat velocity changes slowly during the shock process, which can effectively reduce the shock on the seated occupants, as seen from Figure 15(a).

Observing Figure 15(b), at the beginning, the desired damping force of hybrid controller follows the desired damping force of the vibration controller, which indicates the system is in the state of the vibration control. At the moment of t_M, the desired damping force of hybrid controller follows the desired damping force of shock controller, which indicates the system is in the state of the shock control. Subsequently, the system enters the vibration control at the moment of t_N, which manifests the three phases of shock control are over. Combining with Figure 15(a), the shock excitation occurs at the time of t_M and terminates at the time of

t_N, which indicates that the *Judgment* shown in Figure 5 will achieve the purpose of switching the two controllers.

It can be seen from Figure 15(c) that the MREA can generally output the desired damping force from the controller. Obviously, as seen from Figure 15(d), in the shock control, the seat suspension has undergone three phases of the compression, the rebound, and the second compression. The seat suspension travel stroke is fully utilized. Minor imperfection is that during the seat suspension compression of the first phase, the seat suspension travel stroke is not completely used up. The reason can be found from Figure 15(c) that the tracking damping force of MREA is slightly larger than the desired damping force of the controller. To precisely output the damping force of the MREA is the key to the MR semi-active shock mitigation control systems based on the analysis of the imperfection of the control performance.

As seen from Figure 15(e), the vibration control and shock control are well connected, and there is no sudden change in the accelerations at the controller switching point. It also shows the possibility and effectiveness of the hybrid controller for both shock and vibration mitigation.

6. Conclusion

This article proposed an MR semi-active seat suspension system that can reduce both vibration and blast-induced shock transmitted to the seated occupants. The proposed MR semi-active seat suspension system consists of a coil spring supporting the seat and the occupant, an MREA, and a fail-safe EA rod. The dynamic model of the seat suspension system with a 4-degree-of-freedom lumped-parameter model for seated occupants was established for response analysis of the seat and the parts of human body in the processes of vibration and shock control. A hybrid controller composed of a vibration controller, a shock controller, and a *Judgment* unit for switching the sub-controllers was proposed for both vibration and shock mitigation. The skyhook control strategy was adopted to achieve vibration control and the "soft-landing" control strategy to shock control, and the *Judgment* switches the two control strategies according to the real-time excitation and the response of the seat. A feedforward tracking control strategy based on the basic RC operator hysteresis model was proposed to efficiently provide the MREA damping force. The linearization of the desired damping force of the hybrid controller and the tracking damping force of the MREA was realized. Based on the research results, the following concluding remarks could be drawn:

1. The skyhook controller could provide a better vibration attenuation performance, as compared to the passive systems. But the vibration controller is not suitable for shock mitigation, because unacceptable deceleration or end-stop impact may happen to destroy the payload or system structure.
2. The shock controller based on the concept of "soft-landing," making full of the seat suspension travel stroke and avoiding the end-stop impact, could realize the minimization of the deceleration of the payload. The proposed shock controller shows the following advantages: (a) the desired damping force can be adjusted itself based on the mass of the seated occupants, (b) the desired damping force can be updated in real time based on the system states, and (c) error between the tracking damping force and the desired damping force can be compensated in real time.
3. The *Judgment* unit of the hybrid controller could switch the two sub-controllers during complex excitation. Optimal control performance could not be achieved unless the vibration controller and shock controller work collaboratively.
4. The proposed feedforward tracking control strategy based on the basic RC operator hysteresis model can accurately track desired damping force. In the case of the residual damping forces of the MREA, slight tracking error inevitably

occurs. How to precisely control the output of the strong nonlinear MREAs should still be one of the core issues in shock mitigation systems.

The proposed MR semi-active seat suspension system for the special vehicles and the corresponding hybrid controller investigated in this article establish the foundations for more in-depth researches of the specific applications. Prototyping and experimental tests of the MR semi-active seat suspension system with a seated occupant and also the control strategies will be given in the near future.

ORCID iD

Xian-Xu 'Frank' Bai ⓘ https://orcid.org/0000-0003-4477-8335

References

Bai XX, Cai FL and Chen P (2019) Resistor-capacitor (RC) operator-based hysteresis model for magnetorheological (MR) dampers. *Mechanical Systems and Signal Processing* 117: 157–169.

Bai XX, Chen P and Qian LJ (2015) Principle and validation of modified hysteretic models for magnetorheological dampers. *Smart Materials and Structures* 24(8): 085014.

Bai XX, Jiang P and Qian LJ (2017a) Integrated semi-active seat suspension for both longitudinal and vertical vibration isolation. *Journal of Intelligent Material Systems and Structures* 28(8): 1036–1049.

Bai XX, Wereley NM and Wang DH (2017b) Control and analysis of a magnetorheological energy absorber for both shock and vibration. *International Journal of Acoustics & Vibration* 22(1): 104–110.

Bai XX, Xu SX, Cheng W, et al. (2017c) On 4-degree-of-freedom biodynamic models of seated occupants: lumped-parameter modeling. *Journal of Sound and Vibration* 402: 122–141.

Chen P, Bai XX, Qian LJ, et al. (2018) An approach for hysteresis modeling based on shape function and memory mechanism. *IEEE/ASME Transactions on Mechatronics* 23(3): 1270–1278.

Choi SB and Han YM (2007) Vibration control of electrorheological seat suspension with human-body model using sliding mode control. *Journal of Sound and Vibration* 303(1–2): 391–404.

Choi SB, Nam MH and Lee BK (2000) Vibration control of a MR seat damper for commercial vehicles. *Journal of Intelligent Material Systems and Structures* 11(12): 936–944.

Choi YT and Wereley NM (2005) Mitigation of biodynamic response to vibratory and blast-induced shock loads using magnetorheological seat suspensions. *Proceedings of the Institution of Mechanical Engineers, Part D: Journal of Automobile Engineering* 219(6): 741–753.

Du H, Li W and Zhang N (2011) Semi-active variable stiffness vibration control of vehicle seat suspension using an MR elastomer isolator. *Smart Materials and Structures* 20(10): 105003.

Du XM, Yu M, Fu J, et al. (2018) H∞ control for a semi-active scissors linkage seat suspension with magnetorheological damper. *Journal of Intelligent Material Systems and Structures* 30: 708–721.

Els PS, Theron NJ, Uys PE, et al. (2007) The ride comfort vs. handling compromise for off-road vehicles. *Journal of Terramechanics* 44(4): 303–317.

Hiemenz GJ, Choi YT and Wereley NM (2007) Semi-active control of vertical stroking helicopter crew seat for enhanced crashworthiness. *Journal of Aircraft* 44(3): 1031–1034.

Hui CWZ (2011) Coordinated control of vehicle ride comfort and handling stability based on state identification. *Journal of Mechanical Engineering* 6: 22.

ISO (1997) Mechanical vibration and shock: evaluation of human exposure to whole-body vibration, part 1, general requirements. ISO 2631-1: 1997.

Karnopp D, Crosby MJ and Harwood RA (1974) Vibration control using semi-active force generators. *Journal of Engineering for Industry* 96(2): 619–626.

Li W, Zhang X and Du H (2012) Development and simulation evaluation of a magnetorheological elastomer isolator for seat vibration control. *Journal of Intelligent Material Systems and Structures* 23(9): 1041–1048.

Nieto AJ, Morales AL, Chicharro JM, et al. (2016) An adaptive pneumatic suspension system for improving ride comfort and handling. *Journal of Vibration and Control* 22(6): 1492–1503.

Ning D, Sun S, Du H, et al. (2018) Control of a multiple-DOF vehicle seat suspension with roll and vertical vibration. *Journal of Sound and Vibration* 435: 170–191.

Ning D, Sun S, Zhang J, et al. (2016) An active seat suspension design for vibration control of heavy-duty vehicles. *Journal of Low Frequency Noise, Vibration and Active Control* 35(4): 264–278.

Patil MK and Palanichamy MS (1988) A mathematical model of tractor-occupant system with a new seat suspension for minimization of vibration response. *Applied Mathematical Modelling* 12(1): 63–71.

Phu DX, An JH and Choi SB (2017) A novel hybrid adaptive controller and implementation to vibration control of vehicle seat suspension with MR damper. *Applied Science* 7(10): 1055.

Phu DX, Huy TD, Mien V, et al. (2018a) A new composite adaptive controller featuring the neural network and prescribed sliding surface with application to vibration control. *Mechanical Systems and Signal Processing* 107: 409–428.

Phu DX, Quoc Hung N and Choi SB (2018b) A novel adaptive controller featuring inversely fuzzified values with

application to vibration control of magneto-rheological seat suspension system. *Journal of Vibration and Control* 24(21): 5000–5018.

Phu DX, Shin DK and Choi SB (2015) Design of a new adaptive fuzzy controller and its application to vibration control of a vehicle seat installed with an MR damper. *Smart Materials and Structures* 24(8): 085012.

Radonić V, Barić D, Petricević A, et al. (1994) Military injuries to the popliteal vessels in Croatia. *The Journal of Cardiovascular Surgery* 35(1): 27–32.

Radonić V, Giunio L, Biočić M, et al. (2004) Injuries from antitank mines in Southern Croatia. *Military Medicine* 169(4): 320–324.

Shin DK, Phu DX, Choi SM, et al. (2016) An adaptive fuzzy sliding mode control of magneto-rheological seat suspension with human body model. *Journal of Intelligent Material Systems and Structures* 27(7): 925–934.

Singh HJ and Wereley NM (2014) Optimal control of gun recoil in direct fire using magnetorheological absorbers. *Smart Materials and Structures* 23(5): 055009.

Sun SS, Ning DH, Yang J, et al. (2016) A seat suspension with a rotary magnetorheological damper for heavy duty vehicles. *Smart Materials and Structures* 25(10): 105032.

Sun SS, Yang J, Deng HX, et al. (2015) Horizontal vibration reduction of a seat suspension using negative changing stiffness magnetorheological elastomer isolators. *International Journal of Vehicle Design* 68(1–3): 104–118.

Sun W, Li J, Zhao Y, et al. (2011) Vibration control for active seat suspension systems via dynamic output feedback with limited frequency characteristic. *Mechatronics* 21(1): 250–260.

Uys PE, Els PS and Thoresson M (2007) Suspension settings for optimal ride comfort of off-road vehicles travelling on roads with different roughness and speeds. *Journal of Terramechanics* 44(2): 163–175.

Wang C, Zhang X, Guo K, et al. (2016) Hierarchical optimisation on scissor seat suspension characteristic and structure. *Vehicle System Dynamics* 54(11): 1538–1553.

Weber F (2013) Bouc–Wen model-based real-time force tracking scheme for MR dampers. *Smart Materials and Structures* 22(4): 045012.

Wen YK (1976) Method for random vibration of hysteretic systems. *Journal of the Engineering Mechanics Division* 102(2): 249–263.

Wereley NM, Choi YT and Singh HJ (2011) Adaptive energy absorbers for drop-induced shock mitigation. *Journal of Intelligent Material Systems and Structures* 22(6): 515–519.

Wu X and Griffin MJ (1997) A semi-active control policy to reduce the occurrence and severity of end-stop impacts in a suspension seat with an electrorheological fluid damper. *Journal of Sound and Vibration* 203(5): 781–793.

Yu J, Dong X, Zhang Z, et al. (2018) A novel scissor-type magnetorheological seat suspension system with self-sustainability. *Journal of Intelligent Material Systems and Structures* 30: 665–676.

Zhao Y, Zhao L and Gao H (2010) Vibration control of seat suspension using H∞ reliable control. *Journal of Vibration and Control* 16(12): 1859–1879.

Zuo L and Zhang PS (2013) Energy harvesting, ride comfort, and road handling of regenerative vehicle suspensions. *Journal of Vibration and Acoustics* 135(1): 011002.